Time development of a persistent hole burning in multiple-scattering media

doi: 10.1103/PhysRevE.70.046606

Time development of a persistent hole burning in multiple-scattering media

Makoto Tomita, Kentarou Ono, and Shuho Tatsuno
Department of Physics, Faculty of Science, Shizuoka University, 836, Ohya, Shizuoka 422-8529, Japan
(Received 20 April 2004; published 20 October 2004)

We investigated the time development of persistent hole burning in photoreactive and multiple-scattering media. In this hole burning, a writing laser beam recodes the volume speckle pattern inside the medium through the photoreactive process, and then the luminescence intensity excited by a reading beam is measured as a function of the frequency or wave vector difference between the writing and reading beams. The time development reflects the statistics of the intensity fluctuations in the speckle inside the medium. One of the striking results is that the maximum hole depth is ~0.26. We distinguish three types of samples according to the geometric configurations and the photoreactive processes and discuss the hole shape, hole width, and the depth during time development. Hole burning experiments were also performed using a spiropyran derivative photochromic dye. The experimental results showed good agreement with the theory.

DOI: 10.1103/PhysRevE.70.046606 PACS number(s): 42.25.Dd, 42.30.Ms, 42.70.Mp

I. INTRODUCTION

When a coherent light wave propagates through a multiple-scattering medium, large fluctuations appear as a result of random interference of scattered waves [1,2]. In optics, this phenomenon is known as speckle. Speckle and correlation effects have been utilized in a wide range of fundamental and application measurements. It has been suggested that measurements of the transmission fluctuations provide a decisive test for photon localization in disordered media even in the presence of absorption [3], and the localization of microwaves has been investigated in a quasi-one-dimensional sample [4]. It is theoretically predicted that speckle is sensitive to the scattering potential in a nonlinear medium [5]. Speckle has also been observed in the near field region [6]. In all the traditional speckle correlation measurements, a single laser beam is used. That is, the laser beam is irradiated onto the scattering medium and a reference speckle pattern is recorded once outside the sample. Then the signal speckle is measured after the experimental condition has been slightly shifted and the mutual correlation between the two patterns is numerically calculated on a computer. On the other hand, if one utilizes nonlinear optical effects, one can examine speckle fluctuations inside the medium. The second harmonic intensity generated by two angular correlated excitation laser beams was examined in a multiple-scattering medium consisting of $LiNbO_3$ microparticles [7]. It has been experimentally demonstrated that the second harmonic intensity shows a correlation peak as a function of the angle between the two beams. This observation can be understood as the effect of constructive interference between two speckle patterns generated inside the medium.

Another method to examine the speckle correlation inside the medium may be hole burning in photoreactive and multiple-scattering media. The first observation of such persistent hole burning in collective scatterers may go back to Ref. [8]. Although the experiment in Ref. [8] was motivated to utilize the whispering gallery modes of spheres, the results might have some characteristics relevant to speckles. In hole burning, first, a strong writing beam with incident frequency ω_W and wave vector k_W is injected into the multiple-scattering medium. This beam produces a random interference pattern, i.e., a speckle pattern inside the medium. This speckle pattern is recorded inside the medium through the photoreactive process. After the pattern is recorded, the luminescence intensity from the sample excited by a reading beam of ω_R and k_R is measured as a function of $\Delta\omega=\omega_W-\omega_R$ or $\Delta k=k_W-k_R$. When the frequency and the wave vector of the writing and the reading beams are the same, the spatial fluctuation patterns produced by the two beams also coincide with respect to each other. The reading beam then excites only the photobleached parts of the medium, and the luminescence intensity is reduced. We observe a hole in the luminescence intensity as a function of $\Delta\omega$ or Δk [8–10]. Although the basic mechanism is totally different from the traditional persistent hole burning in a low temperature glassy material [11], hole burning in multiple-scattering media could also have great potential for multiwavelength optical data storage.

In a previous paper, we analyzed the hole burning effect on the basis of the intensity correlation between the writing and reading beams inside the medium and examined the dependence of the hole shape and width on the sample thickness, transport mean free path, geometric configuration, and absorption effects [9]. One of the striking differences between the second harmonic correlation measurement and the hole burning effect may be that in the hole burning experiments the saturation effect or a higher order effect of the speckle appears very easily. A well developed speckle has statistical fluctuations in the intensity that obey a single exponential distribution, i.e., $\exp(-I/\langle I\rangle)$, where $\langle I\rangle$ is the average intensity. The photoreaction proceeds slowly at local places inside the medium where the speckle intensity is weak. On the other hand, saturation occurs very easily at places where the local intensity is strong, since the development of the photoreaction is relevant to the total photon number injected. The time development, therefore, reflects the statistically fluctuating intensity of the speckle inside the medium.

In the present paper, we investigate the time development of hole burning in a photoreactive and multiple-scattering medium. One of the striking results is that there exists a maximum hole depth of ~0.26. The hole depth may be a crucial parameter when one considers real applications of hole burning in optical devices. We consider three types of photoreactive and multiple-scattering media and examine the hole shape, hole width, and depth during time development. First, we theoretically examine the time development. Then we also present hole burning experiments using a spiropyran derivative photochromic dye as the photoreactive material in order to confirm the theory.

II. LOCAL CORRELATION, INTENSITY AND PROPAGATOR

The electric fields at the incident surface of the medium are represented as

$$E_i(R) = E_{i_0} \exp[-i(\omega_i t - k_i R)], \tag{1}$$

where the subscript i is W and R for the writing and reading beams, respectively, and R is the transverse vector at the incoming surface. $I_{i_0}=|E_{i_0}|^2$ is the intensity of the incident laser beam. The light propagates in the medium, undergoing multiple scattering, and appears as the local electric field $E_{i\ local}(r)$ inside the medium,

$$E_{i\ local}(r) = \int_{surface} dR \sum_{\xi=all} W_\xi(r,R) E_i(R), \tag{2}$$

where $W_\xi(r,R)$ is the probability amplitude that the field propagates from R to r along a trajectory ξ, and the summation $\Sigma_{\xi=all}$ is taken over all possible trajectories. We consider that the photoreaction develops proportionally to the local intensity of the writing beam,

$$\frac{dN_f(r)}{dt} = -\eta_\alpha \eta_p I_{W\ local}(r) N_f(r), \tag{3}$$

where $N_f(r)$ is the number of fresh luminescence centers, η_a is the absorption cross section, η_p is the efficiency of the photoreaction, and $I_{W\ local}(r)$ is the local intensity of the writing beam. The number of fresh centers at a time t after the laser irradiation is

$$N_f(t,r) = N_0 \exp[-\eta_\alpha \eta_p I_{W\ local}(r) t], \tag{4}$$

where N_0 is the total number of luminescence centers. We consider that the luminescence light is emitted only from the fresh centers, while the photoreacted centers do not emit. The total luminescence intensity from the medium excited by the reading beam may be

$$H(R_d) = K \int \langle N_f(r) I_{R\ local}(r) \rangle T(r,R_d) dr, \tag{5}$$

where the angular brackets $\langle\ \rangle$ represent the ensemble average for the random configuration of the scatterers, $I_{R\ local}(r)$ is the local intensity of the reading beam, $T(r,R_d)$ is the propagator for the luminescence light from r inside the medium to the detection point R_d, and K is a constant to represent the detection efficiency. Substituting Eq. (4) into Eq. (5), we obtain

$$\begin{aligned} H(R_d) &= K \int \langle N_0 \exp[-\kappa I_{W\ local}(r)] I_{R\ local}(r) \rangle T(r,R_d) dr \\ &= K \int \left\langle N_0 \left(1 - \kappa I_{W\ local}(r) + \frac{1}{2!}[\kappa I_{W\ local}(r)]^2 \right.\right. \\ &\quad \left.\left. - \frac{1}{3!}[\kappa I_{W\ local}(r)]^3 + \cdots \right) I_{R\ local}(r) \right\rangle T(r,R_d) dr, \end{aligned} \tag{6}$$

where $\kappa = \eta_a \eta_p t$. Under the condition that $\kappa I_{W\ local} \ll 1$, that is, the writing time is short, the expansion can be terminated at first order. We obtain

$$H(R_d) = K \int N_0 \kappa \langle I_{W\ local}(r) I_{R\ local}(r) \rangle T(r,R_d) dr. \tag{7}$$

This situation corresponds to the previous analysis of the hole burning in a photoreactive and multiple-scattering medium. In this situation, the hole is described on the basis of the local intensity correlation of the writing and reading beams. We have analyzed the dependence of the hole shape and the hole width on sample thickness, transport mean free path, geometrical configuration, and absorption lengths in Ref. [9].

Now we take the higher-order terms into account. The nth-order term in the writing beam intensity is

$$\langle I^n_{W\ local} I_{R\ local} \rangle = \langle (E_{W\ local} E^*_{W\ local})^n E_{R\ local} E^*_{R\ local} \rangle. \tag{8}$$

In optical experiments in a slab geometry the contributions of the long and infinite range correlations are negligible [12], and we assume that the fluctuations obey circular Gaussian statistics [13]. The nth-order moment can be divided into sum of the products of the second-order moment. There are $(n-1)!$ combinations of the electric fields of the writing beam,

$$\begin{aligned}
&\langle (E_{W\ local}E^{*}_{W\ local})^{n}E_{R\ local}E^{*}_{R\ local}\rangle \\
&\quad = (n-1)!\langle E_{W\ local}E^{*}_{W\ local}\rangle^{n}\langle E_{R\ local}E^{*}_{R\ local}\rangle \\
&\qquad + (n-1)(n-1)!\langle E_{W\ local}E^{*}_{W\ local}\rangle^{n-2}|\langle E_{W\ local}E^{*}_{R\ local}\rangle \\
&\qquad \times\langle E_{R\ local}E^{*}_{W\ local}\rangle| \\
&\quad = (n-1)!I^{n}_{W\ local}I_{R\ local} + (n-1)(n-1)!I^{n-2}_{W\ local} \\
&\qquad \times|\langle E_{W\ local}E^{*}_{R\ local}\rangle|^{2}. \qquad (9)
\end{aligned}$$

It is noted that the electric field correlation between the writing and reading beams appears only at the second order even in the higher-order correlation terms. Combining Eq. (6) with Eq. (9), we obtain

$$\begin{aligned}
&\langle N_0 \exp[-\kappa I_{W\ local}(r)]I_{R\ local}(r)\rangle \\
&\quad = N_0\left(\frac{\langle I_{R\ local}(r)\rangle}{[1+\kappa\langle I_{W\ local}(r)\rangle]} - \frac{\kappa}{[1+\kappa\langle I_{W\ local}(r)\rangle]^{2}}\right. \\
&\qquad \left.\times|\langle E_{W\ local}(r)E^{*}_{R\ local}(r)\rangle|^{2}\right). \qquad (10)
\end{aligned}$$

From Eqs. (1) and (2), we obtain

$$\begin{aligned}
C(r,\Delta\omega,\Delta k) &= |\langle E_{W\ local}(r)E^{*}_{R\ local}(r)\rangle|^{2} \\
&= I_{W_0}I_{R_0}\int_{\text{surface}} dR_{\xi_1}\int dR_{\xi_2}\sum_{\xi_1}\sum_{\xi_2}|W_{\xi_1}(r,R_{\xi_1})|^{2} \\
&\quad \times|W_{\xi_2}(r,R_{\xi_2})|^{2}\exp[-i\{\Delta\omega/c(s_{\xi_1}-s_{\xi_2}) \\
&\quad - \Delta k(R_{\xi_1}-R_{\xi_2})\}], \qquad (11)
\end{aligned}$$

where s_ξ is the length of the trajectory ξ. Let us consider a slab sample with a thickness of L. We consider a situation where the size of the incident laser beams is larger than L and calculate the time development of the hole. We assume that the absorption lengths for the writing and the reading beams are the same, since the frequency difference between the two beams is generally small compared with the absorption band of the photoreactive material. The absorption length for the luminescence light could be different from the writing and reading beams owing to the large Stokes shift in the photoluminescence process. The diffusive absorption lengths are denoted as $L_a=\alpha^{-1}=(l^{*}l_a/3)^{1/2}$ and $L_{la}=\alpha_{la}{}^{-1}=(l^{*}l_{la}/3)^{1/2}$, where l_a and l_{la} are the absorption lengths for the writing and reading beams and for the luminescence light, respectively, and l^{*} is the transport mean free path. The procedure to calculate the local correlation function is the same as that used in the previous paper [9]. In order to calculate the sum of trajectories in Eq. (11), we replace the summation with an integration over the distribution function of the trajectories, $\Sigma|W|^{2}\rightarrow\int dRds\mathrm{P}(r,R,s)$, where s is the trajectory length and R is the transverse vector parallel to the incident surface. The distribution function of the trajectories is calculated on the basis of the diffusion approximation. The z axis is taken to be perpendicular to the incident surface, and we set the absorbing wall at $z=-C$ and $L+C$, where $C=(2l^{*}/3)(1+\rho)/(1-\rho)$ is the explanation distance and ρ the internal reflection coefficient. When the internal reflection is negligible, the exportation distance is $C=0.701l^{*}$. The correlation function is obtained as

$$\begin{aligned}
&C(z,\Delta\omega,\Delta k) \\
&\quad = I_{W_0}I_{R_0}\frac{\cosh[2\gamma(L+C-z)]-\cos[2\delta(L+C-z)]}{\cosh[2\gamma(L+2C)]-\cos[2\delta(L+2C)]}, \qquad (12)
\end{aligned}$$

where $\beta=\gamma+i\delta=\sqrt{\Delta k^{2}+(1/\tau_a+i\Delta\omega)/D}$, $\tau_a=l_a/c$, c is the velocity of light inside the medium, and D is the diffusion constant. The propagator $T(r,R_d)$ is also calculated on the basis of the diffusion approximation,

$$\begin{aligned}
T(z,z_d) &= \int dR_d T(r,R_d) \\
&= \frac{\sinh[(z_1+C)/L_{la}]\sinh[(L+C-z_2)/L_{la}]}{1/L_{la}\sinh[(L+2C)/L_{la}]}, \qquad (13)
\end{aligned}$$

where $z_1=z$, $z_2=z_d=L-l^{*}$ for the transmission geometry, and $z_1=z_d=l^{*}$, $z_2=z$ for the reflection geometry. The local intensities of the writing and the reading beams are

$$I_{i\ local}(z) = I_{i_0}\frac{\sinh[(L+C-z)/L_a]}{\sinh[(L+2C)/L_a]}. \qquad (14)$$

Substituting Eqs. (12)–(14) into Eq. (5), we obtain the form factor for the time development of the hole in the photoreactive and multiple-scattering medium.

III. TIME DEVELOPMENT OF THE HOLE

In the present paper, we distinguish three types of photoreactive and multiple-scattering media, according to the geometric configurations and the photoreactive processes, and discuss the hole shape, hole width, and depth.

The type I sample consists of a slab of a multiple-scattering medium on which a photoreactive film is coated. In this sample, the multiple-scattering medium is responsible for the speckle formation, while the photoreactive film is responsible for the recording process of the speckle pattern at the outgoing surface. The type I sample is the simplest system to examine the time development of hole burning by a statistically fluctuating speckle intensity. We may experimentally confirm the validity of the theoretical treatment of Eq. (6) in a simple and clear manner in the type I sample. The multiple scattering or the volume speckle is, however, not essential in this sample, since the photoreactive film records only the speckle on the outgoing surface. From the application point of view, the type I sample may, however, be useful because we can obtain the narrow spectral and angular holes compared with the type II and III samples discussed below.

In the type I sample, the analysis is straightforward. In this case, we set $z=L$ in Eqs. (12)–(14), respectively. Using Eq. (10), we obtain

$$H_I(\kappa,\Delta k,\Delta\omega)=N_0\left(\frac{\langle I_{R\ local}(L)\rangle}{[1+\kappa\langle I_{W\ local}(L)\rangle]}-\frac{\kappa}{[1+\kappa\langle I_{W\ local}(L)\rangle]^2}\frac{\cosh(2\gamma C)-\cos(2\delta C)}{\cosh[2\gamma(L+2C)]-\cos[2\delta(L+2C)]}\right). \tag{15}$$

The luminescence intensities at the hole center $H_I(\kappa,0,0)$ and at the background level $H_I(\kappa,\infty,\infty)$ are obtained as

$$H_I(\kappa,0,0)=\frac{N_0\langle I_{R\ local}(L)\rangle}{[1+\kappa\langle I_{W\ local}(L)\rangle]^2}, \tag{16}$$

and

$$H_I(\kappa,\infty,\infty)=\frac{N_0\langle I_{R\ local}(L)\rangle}{[1+\kappa\langle I_{W\ local}(L)\rangle]}, \tag{17}$$

respectively. The time dependence is included through $\kappa=\eta_a\eta_p t$. The hole depth can be defined as $H_{dep}(\kappa)=H(\kappa,\infty,\infty)-H(\kappa,0,0)$. It is noted that the luminescence intensities at the hole center and at the background level decrease monotonically, whereas the hole depth initially increases, then saturates, and decreases when $\kappa\langle I_{W\ local}\rangle>1$. The maximum hole depth is ~ 0.26. The physical origin of the shallow hole is explained as follows. The basic mechanism of the hole burning is the recording process of the speckle pattern. A well developed speckle has statistical fluctuations in the intensity that obey a single exponential distribution, i.e., $\exp(-I/\langle I\rangle)$ [1]. At the initial stage of the hole burning, the photoreaction proceeds at the local places where the speckle intensity is strong. With increasing writing time, the reaction proceeds successively at the local places where the specked intensity is weak, while the saturation occurs at the places where the intensity is strong. The saturation effect destroys the recorded spatial pattern; therefore, further irradiation of the writing beam contributes only to the background level. From Eqs. (16) and (17), it is also seen that the ratio of the hole depth to the background level is $H_{Idep}(\kappa)/\{1-H_I(\kappa,\infty,\infty)\}=1/1$ at the initial stage of the hole burning. In contrast to the type II and the type III samples discussed below, the width of the hole is constant during the hole burning process in the type I sample as is seen in Eq. (15).

Type II and type III samples are multiple-scattering media in which photoreactive material is uniformly dispersed. The type II and type III samples are distinguished according to the difference in the photoreaction. In the type II sample, we consider a photoreaction in which the absorption spectrum as well as the absorption coefficient is unchanged, while the luminescence intensity decreases. Luminescence fatigue or various kinds of photoinduced physical and chemical processes may be classified into this category. In the previous hole burning experiments, we used microparticles of CdS_xSe_{1-x}-doped glass [9]. The photoluminescence of this glass shows fatigue under strong laser irradiation, while the absorption spectrum and the coefficient are constant during this fatigue process [14]. On the other hand, in the type III sample, we consider a photoreaction in which the absorption spectrum and the coefficient change under laser irradiation. A photochromic dye, which is used in Sec. IV, is an example. Typically, an absorption band in the visible region appears after irradiation of ultraviolet (uv) light. This absorption band disappears under the irradiation of visible light. These processes are usually stable and repeatable. With the type II and the type III samples, we can examine the time development of the hole in multiple-scattering media. In contrast to the traditional speckle measurements, where the real speckle patterns are observed outside the sample, we can obtain information on the fluctuations and the correlations inside the multiple-scattering medium using type II and type III samples.

In the type II sample, the absorption is constant during the photoreaction. Therefore, the optical trajectories of the writing beam inside the medium, as well as the local speckle pattern are unchanged, under the time development of the hole burning. Substituting Eqs. (10) and (12)–(14) into (5), we obtain the normalized hole shape

$$\tilde{H}_{II}^{R}(\kappa,\Delta k,\Delta\omega)=\frac{\displaystyle\int_0^L dz\frac{\sinh[(L+C-z)\alpha_{la}]}{\sinh[(L+2C)\alpha_{la}]}\left\{\frac{\sinh[(L+C-z)\alpha]}{\{\sinh[(L+2C)\alpha]+\kappa I_{W\,0}\sinh[(L+C-z)\alpha]\}}\right.}{\displaystyle\int_0^L dz\frac{\sinh[(L+C-z)\alpha]\sinh[(z+C)\alpha_{la}]}{\sinh[(L+2C)\alpha]\sinh[(L+2C)\alpha_{la}]}}$$
$$\left.-\kappa I_{W\,0}\frac{\sinh^2[(L+2C)\alpha]}{\{\sinh[(L+2C)\alpha]+\kappa I_{W\,0}\sinh[(L+C-z)\alpha]\}^2}\left|\frac{\sinh[(L+C-z)\beta]}{\sinh[(L+2C)\beta]}\right|^2\right\}, \tag{18}$$

for the reflection geometry. A similar equation can be obtained for the transmission geometry. The above equations are general formulas, which can be used to calculate the dependencies of the time development on the sample thickness, transport mean free path, and absorption for the excitation and for the luminescence light. In case the absorption is weak $L_a, L_{la}\gg L$ and $L\gg l^*$, we obtain the following equations by performing the integration over z:

$$\tilde{H}_{II}^{T}(\kappa,\Delta k,\Delta\omega{:}L_a,L_{la}\to\infty)$$
$$=\frac{3}{\{\kappa I_{W_0}\}^3}[(\kappa I_{W_0})^2+2\kappa I_{W_0}-2(1+\kappa I_{W_0})\ln(1+\kappa I_{W_0})]-\frac{6}{\kappa I_{W_0}[\cosh(2\gamma)-\cos(2\delta)]}$$
$$\times\left\{\left|\cosh\left(\frac{2\gamma}{\kappa I_{W_0}}\right)\left[-\mathrm{Chi}(x)+\left(\frac{2\gamma}{\kappa I_{W_0}}\right)(1+\kappa I_{W_0})\left(\mathrm{Shi}(x)-\frac{\cosh(x)}{x}\right)\right]\right.\right.$$
$$\left.-\sinh\left(\frac{2\gamma}{\kappa I_{W_0}}\right)\left[-\mathrm{Shi}(x)+\left(\frac{2\gamma}{\kappa I_{W_0}}\right)(1+\kappa I_{W_0})\left(\mathrm{Chi}(x)-\frac{\sinh(x)}{x}\right)\right]\right|_{2\gamma/\kappa I_{W_0}}^{(2\gamma/\kappa I_{W_0})(1+\kappa I_{W_0})}$$
$$+\left|-\cos\left(\frac{2\delta}{\kappa I_{W_0}}\right)\left[-\mathrm{Ci}(x)+\left(\frac{2\delta}{\kappa I_{W_0}}\right)(1+\kappa I_{W_0})\left(-\mathrm{Si}(x)-\frac{\cos(x)}{x}\right)\right]\right.$$
$$\left.\left.-\sin\left(\frac{2\delta}{\kappa I_{W_0}}\right)\left[-\mathrm{Si}(x)+\left(\frac{2\delta}{\kappa I_{W_0}}\right)(1+\kappa I_{W_0})\left(\mathrm{Ci}(x)-\frac{\sin(x)}{x}\right)\right]\right|_{2\delta/\kappa I_{W_0}}^{(2\delta/\kappa I_{W_0})(1+\kappa I_{W_0})}\right\},\tag{19}$$

and

$$\tilde{H}_{II}^{R}(\kappa,\Delta k,\Delta\omega{:}L_a,L_{la}\to\infty)$$
$$=\frac{3}{2\{\kappa I_{W_0}\}^3}\left[(\kappa I_{W_0})^2-2\kappa I_{W_0}+2\ln(1+\kappa I_{W_0})\right]-\frac{3}{\kappa I_{W_0}[\cosh(2\gamma)-\cos(2\delta)]}$$
$$\times\left\{\left|\cosh\left(\frac{2\gamma}{\kappa I_{W_0}}\right)\left[\mathrm{Chi}(x)+\left(\frac{2\gamma}{\kappa I_{W_0}}\right)\left(-\mathrm{Shi}(x)+\frac{\cosh(x)}{x}\right)\right]\right.\right.$$
$$\left.-\sinh\left(\frac{2\gamma}{\kappa I_{W_0}}\right)\left[\mathrm{Shi}(x)+\left(\frac{2\gamma}{\kappa I_{W_0}}\right)\left(-\mathrm{Chi}(x)+\frac{\sinh(x)}{x}\right)\right]\right|_{2\gamma/\kappa I_{W_0}}^{(2\gamma/\kappa I_{W_0})(1+\kappa I_{W_0})}$$
$$+\left|-\cos\left(\frac{2\delta}{\kappa I_{W_0}}\right)\left[\mathrm{Ci}(x)+\left(\frac{2\delta}{\kappa I_{W_0}}\right)\left(\mathrm{Si}(x)+\frac{\cos(x)}{x}\right)\right]\right.$$
$$\left.\left.-\sin\left(\frac{2\delta}{\kappa I_{W_0}}\right)\left[\mathrm{Si}(x)+\left(\frac{2\delta}{\kappa I_{W_0}}\right)\left(-\mathrm{Ci}(x)+\frac{\sin(x)}{x}\right)\right]\right|_{2\delta/\kappa I_{W_0}}^{(2\delta/\kappa I_{W_0})(1+\kappa I_{W_0})}\right\},\tag{20}$$

for the transmission and the reflection geometry, respectively, where $\mathrm{Si}=\int_0^x\sin(x)/x dx$, Ci, $\mathrm{Shi}=\int_0^x\sinh(x)/x dx$, and Chi are the sine, cosine, hyperbolic sine, and hyperbolic cosine integrals, respectively, and $|F(x)|_a^b=F(b)-F(a)$. In Fig. 1 we plotted the time development of the hole burning in the transmission and the reflection geometries in Δk and $\Delta\omega$ domains in the type II sample. We see that with increasing writing time the hole width becomes slightly narrower. This narrowing is explained as follows. In the vicinity of the incident surface of the sample (in the small z region), the average intensity of the writing beam is strong, which means that the photoreaction proceeds fast and the luminescence intensity contributing to the total hole shape from this region decreases rapidly. Since the correlation function $C(z,\Delta k)$ is broad in the small z region, the width of the hole becomes slightly narrower during the time development. It is noted that in the type II sample the width of the local correlation function $C(z,\Delta k)$ at a fixed z is constant during the time development process, since the absorption and therefore the trajectories of the writing beam and the speckle pattern are unchanged during the time development. Equations (19) and (20) are complicated expressions. More simple and useful results may be the intensity at the hole center and the background level,

$$\tilde{H}_{II}^{T}(\kappa,0,0)=\frac{6}{(\kappa I_{W_0})^3}[-2\kappa I_{W_0}+(2+\kappa I_{W_0})\ln(1+\kappa I_{W_0})],\tag{21}$$

$$\tilde{H}_{II}^{T}(\kappa,\infty,\infty)=\frac{3}{(\kappa I_{W_0})^3}[(\kappa I_{W_0})^2+2\kappa I_{W_0}-2(1+\kappa I_{W_0})\ln(1+\kappa I_{W_0})],\tag{22}$$

for the transmission geometry, and

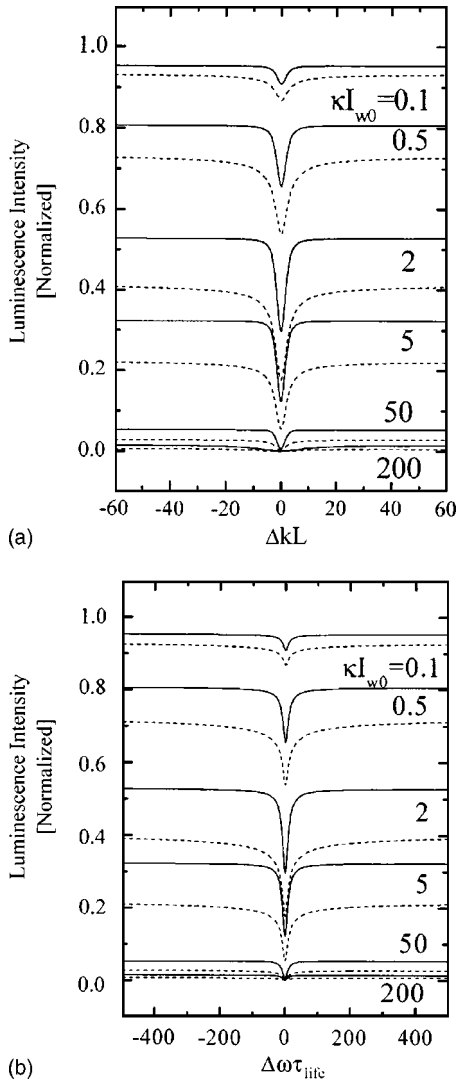

FIG. 1. Calculated curves for the luminescence intensity as a function of (a) ΔkL and (b) $\Delta\omega\tau_{life}$, where $\tau_{life}=L^2/D$, in the type II sample. Solid and dotted lines are for the transmission and the reflection geometries, respectively. From the top to the bottom, $\kappa I_{W_0}=0.1$, 0.5, 2, 5, 50, 200, respectively.

$$\tilde{H}_{II}^{R}(\kappa,0,0)=\frac{3}{(\kappa I_{W_0})^3}\left(\kappa I_{W_0}-2\ln(1+\kappa I_{W_0})+\frac{\kappa I_{W_0}}{\kappa I_{W_0}+1}\right), \tag{23}$$

$$\tilde{H}_{II}^{R}(\kappa,\infty,\infty)=\frac{3}{2(\kappa I_{W_0})^3}[(\kappa I_{W_0})^2-2\kappa I_{W_0}+2\times\ln(1+\kappa I_{W_0})], \tag{24}$$

for the reflection geometry. These expressions will be used in the analysis of the experimental results in Sec. IV.

In the type III sample, the absorption spectrum or the absorption coefficient changes during the photoreaction. In this sample, since the trajectories of the writing beam change during the time development, the speckle pattern inside the medium is no longer constant. The hole shape and hole width

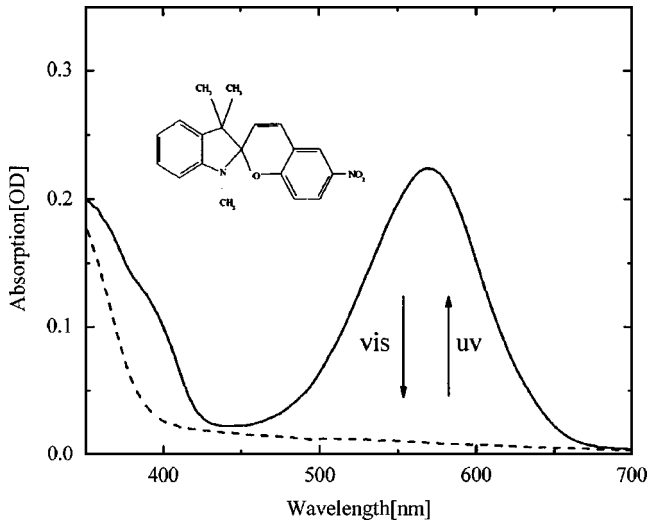

FIG. 2. Absorption spectra of SP-1 in PMMA. Solid line is the initial colored state after uv irradiation. Dashed line is the colorless state after Ar^+ laser irradiation. Inset shows the structural formula of SP1.

are expected to change substantially, owing to the deformation and destruction of the speckle pattern due to the absorption change. The hole could strongly change in the refection geometry compared with the transmission geometry. Analytical solution of the hole shape and width as well as the depth may be complicated in the type III sample. Numerical simulations and further theoretical development are expected. It should be noted that when the absorption in the sample is as weak as $L_a \geqslant L$, even the type III sample can be approximately treated as a type II sample, since the speckle change is small compared with the averaged local intensity.

IV. EXPERIMENTS

We experimentally examined the time development of the hole burning in photoreactive and multiple-scattering media in the Δk domain. We prepared three types of samples. In all samples a spiropyran derivative dye, 1′,3′-dihydro-

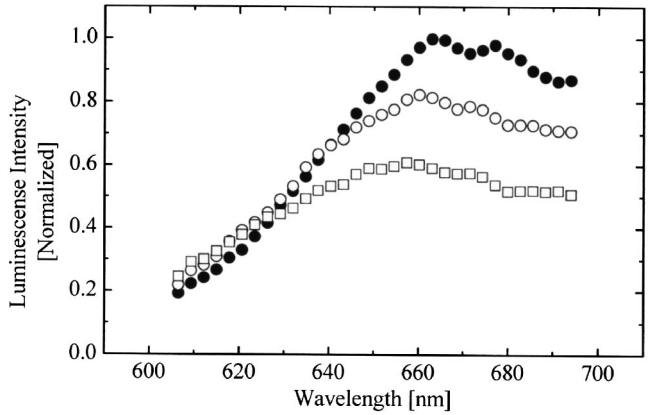

FIG. 3. Solid and open circles and open squares are luminescence spectra of SP1 in PMMA after laser irradiation of 8 s, 30 s, and 53 s, respectively.

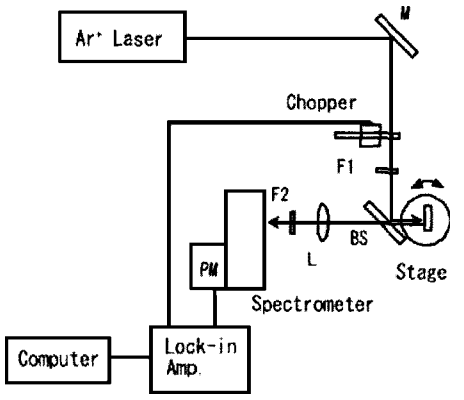

FIG. 4. Schematic illustration of the experimental setup for the hole burning in the reflection geometry. M is the mirror, BS is the beam splitter, L is the lens, F1 and F2 are the filters, and PM is the photomultiplier tube.

1′,2′,3′- trimethyl-6-nitrospiro[2H-1-benzopyran-2,2′-(2H) indole] (SP1) was used as the photoreactive material. This dye shows typical photochromium. Figure 2 shows the absorption spectra of SP1 dye in a polymethylmethacrylate (PMMA) film. The solid line corresponds to the colored state after uv light irradiation. In this state, the sample has an absorption band at 570 nm and appears deep purple in color. The dashed line in Fig. 2 is the colorless state after visible light irradiation, in which the 570 nm absorption band disappears. The luminescence spectra of SP1 in the PMMA film excited by a 514.5 nm Ar^+ laser are shown in Fig. 3. The

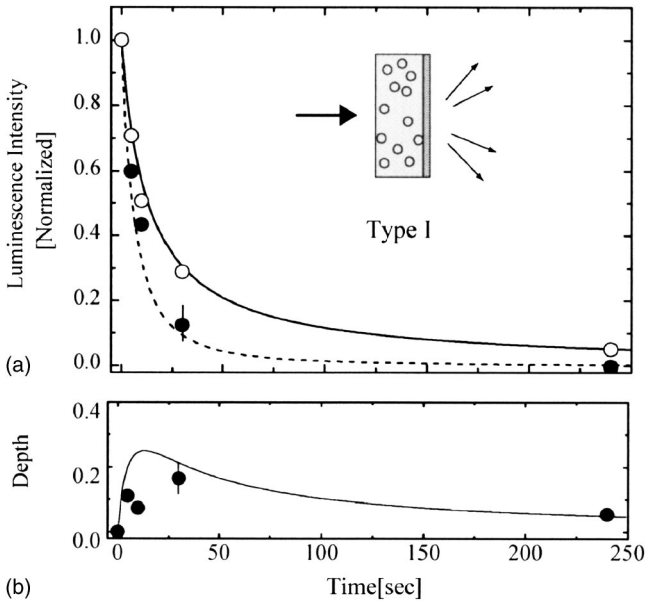

FIG. 5. Experimental results for the time development of the hole burning in the type I sample. (a) Solid and open circles are luminescence intensities at the hole center $\tilde{H}(\Delta k=0)$ and at the background level $\tilde{H}(\Delta k=\infty)$, respectively, as a function of the writing time. The dashed and solid lines are calculated curves on the basis of Eqs. (16) and (17). (b) The solid circles are the hole depths. The inset in (a) is a schematic illustration of the type I sample. The gray region represents the photochromic film.

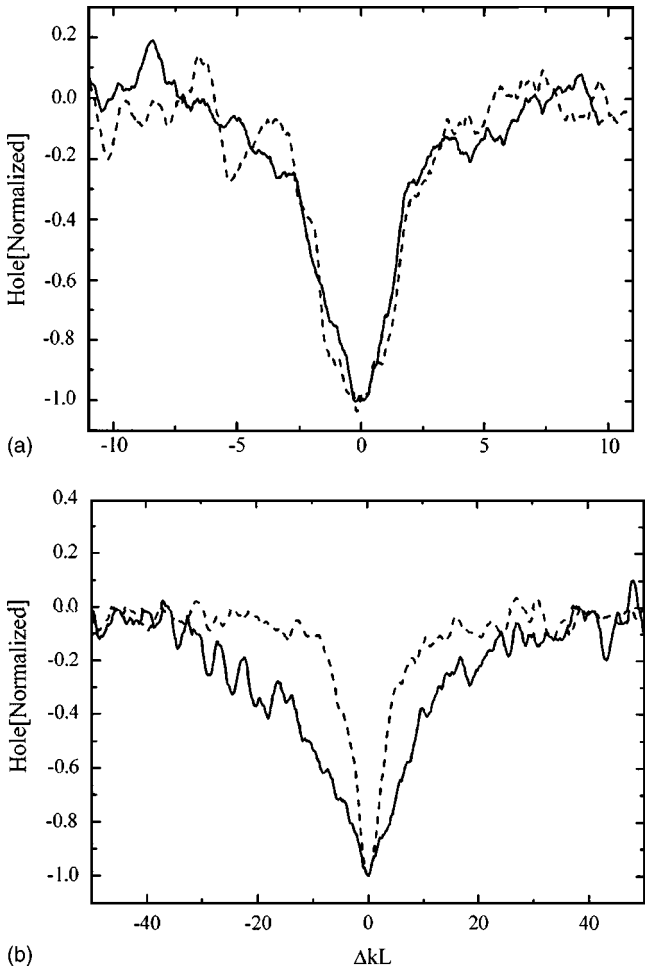

FIG. 6. The normalized holes as a function of ΔkL. (a) is for the type I sample. Solid and dashed lines are $T_W=5$ s and $T_W=240$ s, respectively. (b) is for the type III sample. Solid and dashed lines are $T_W=30$ s and $T_W=7500$ s, respectively.

luminescence spectra show an emission band at 660 nm. With increasing laser irradiation time, the luminescence intensity decreases, which is accompanied by the disappearance of the 570 nm absorption band by visible light irradiation. The luminescence intensity at 660 nm as a function of laser irradiation time can be fitted by a curve $a+b\times\exp(-t/c)$, where a, b, and c are constants. This exponential dependence is reasonable if the time development of the photochromic reaction is proportional only to the total photon number injected. The background level can be attributed to the luminescence due to the residual absorption of the colorless state of SP1 in the PMMA film. In the hole burning experiment described below, we subtracted this background level from the results.

For the type I sample, we first prepared a multiple-scattering medium in a slab geometry, which consists of TiO_2 microparticles suspended in a solid polystyrene host. The average diameter of the TiO_2 microparticles was 0.25 μm and the volume fraction was 3.5%. A thin PMMA film with $7.6\times10^{-2}M$ of SP1 was spin coated on the multiple-scattering medium. The thickness of the multiple-scattering medium and the PMMA film were 0.2 mm and

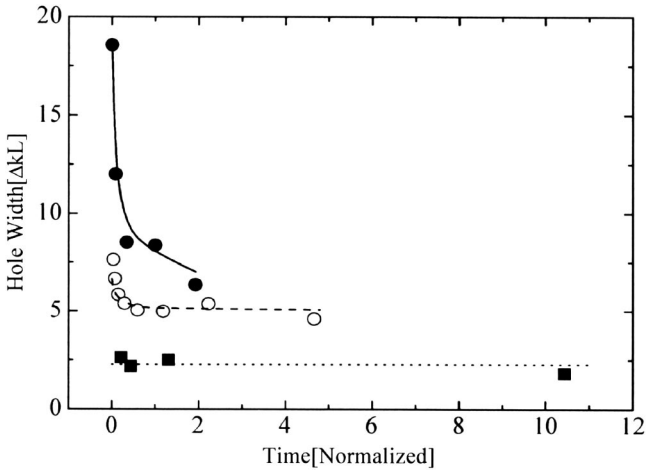

FIG. 7. The normalized holes width $\Gamma_{\Delta k}$ as a function of the normalized writing time. Solid squares and open and solid circles are type I, type II, and type III samples, respectively. The writing time is normalized by the time required for the background level to decrease to $1/e$ of the initial value for each sample. The dotted line represents $\Gamma_{\Delta k}$=const for the type I sample, the dashed line is the calculation from Eq. (18) for the type II sample, and the solid line is a guide for eyes for the type III sample.

~ 5 μm, respectively. The transport mean free path for the 514.5 nm light in the medium was determined to be 31 μm from a total transmission experiment. For the type II and type III samples, we prepared a SP1-doped thin PMMA film and grained this film into micropowders. These powders were compacted into 1 mm thickness between two glass plates and used as the samples. The transport mean free path was 81 μm in the type II and the type III samples. In the type II sample, the dye concentration was $3.9\times10^{-4}M$, which resulted in an absorption length of l_a=2000 μm and the diffusive absorption length L_a=232 μm. In the type III sample, the dye concentration was $4.6\times10^{-2}M$, the absorption length was l_a=16 μm, and the diffusive absorption length was L_a=21 μm. It is noted that in the above type II sample the diffusive absorption length is of the same order as the sample thickness as $L_a\sim L$, whereas in the type III sample $L_a \ll L$. As we discussed in Sec. III, when $L_a \geqslant L$ the type III sample can well be dealt with as a type II sample.

The setup for the hole burning experiments is schematically illustrated in Fig. 4. We used an Ar^+ laser of 514.5 nm for the writing and the reading beams. The sample was set on a stage and rotated by a stepping motor to change the incident angle between the beam and the sample. Before the hole burning experiments, samples were exposed to uv light and prepared in the initial colored state throughout the medium. The uv light was supplied from a 100 W halogen lamp in front of which a uv ($<$360 nm) light pass filter was attached. After the hole burning experiments the samples were in the colorless state and appeared white or light pink in color. First, the laser beam was irradiated on the sample to record the volume speckle pattern through the photochromic process. Then the beam intensity was attenuated by a factor of $\sim$100 and used as the reading beam. The luminescence excited by the reading beam was collected by a lens in both the transmission (not shown in Fig. 4) and the reflection geometries and led into a spectrometer. The luminescence was detected by a photomultiplier tube and measured as a function of the angle of the rotational stage. The photochromic reaction from the colored to the colorless state and the reverse process were stable and repeatable.

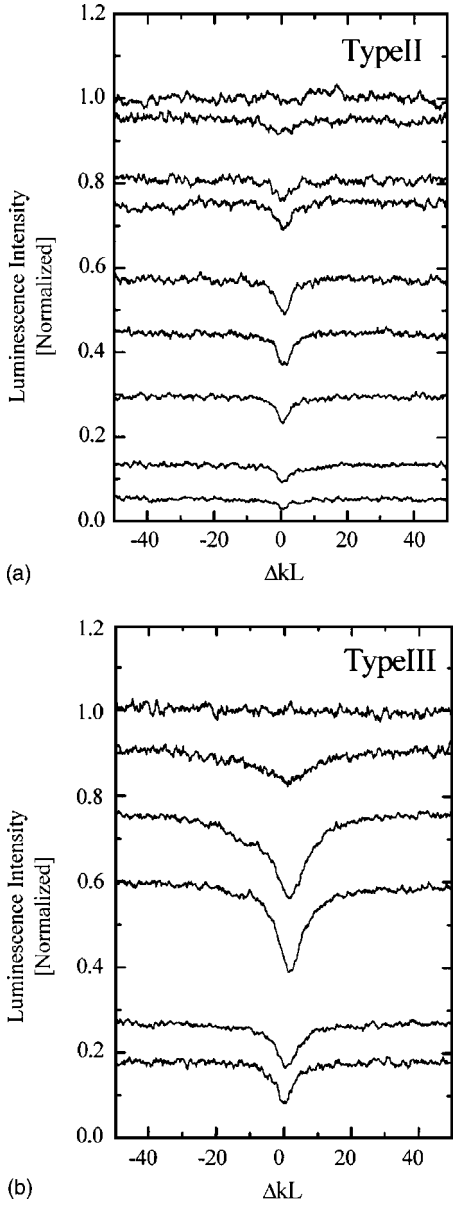

FIG. 8. (a) The luminescence intensity as a function of ΔkL in the type II sample in the reflection geometry. From the top to the bottom, T_W=0, 10, 20, 40, 80, 160, 320, 600, 1260 s, respectively. (b) The luminescence intensity as a function of ΔkL in the type III sample in the reflection geometry. From the top to the bottom, T_W =0, 30, 330, 1350, 3900, 7500 s, respectively.

First, we examined the type I sample. Figure 5 shows the luminescence intensities at the hole center $\tilde{H}_I(\Delta k=0)$ and at the background level $\tilde{H}_I(\Delta k\to\infty)$ as a function of the writing time in the type I sample in the transmission geometry. The

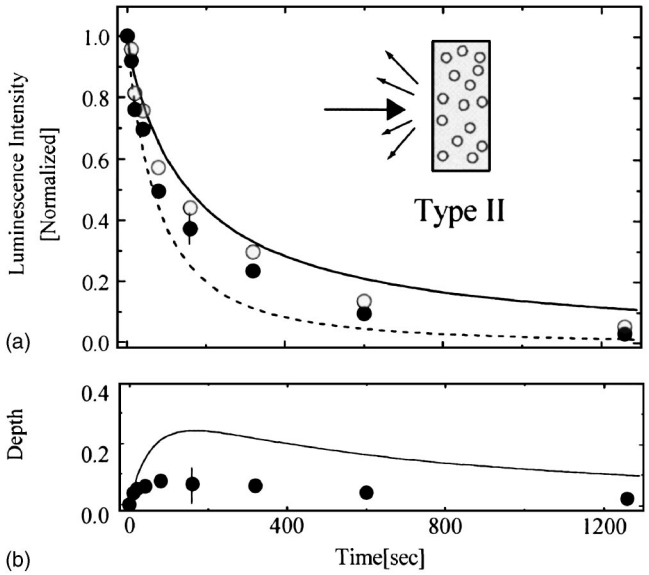

FIG. 9. Experimental results for the time development of the hole burning in the type II sample in the reflection geometry. (a) Solid and open circles represent $\tilde{H}(\Delta k=0)$ and $\tilde{H}(\Delta k=\infty)$, respectively. The dashed and solid lines are calculated curves on the basis of Eqs. (24) and (23). (b) The solid circles represent the hole depth. The inset in (a) shows a schematic illustration of the type II sample.

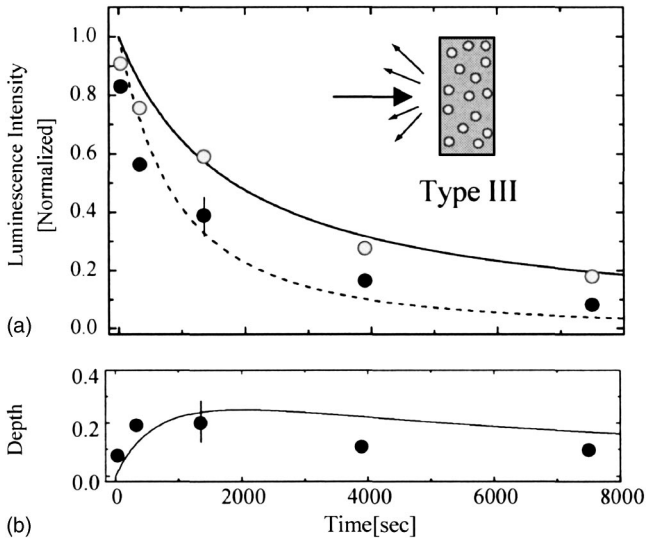

FIG. 10. Experimental results for the time development of the hole burning in the type III sample in the reflection geometry. (a) Solid circles and open circles represent $\tilde{H}(\Delta k=0)$ and $\tilde{H}(\Delta k=\infty)$, respectively. The solid and dashed lines are guides for the eyes. The inset in (a) is a schematic illustration of the type III sample. (b) The solid circles represent the hole depth.

hole depth was defined as $\tilde{H}_{Idep}=\tilde{H}_I(\Delta k\rightarrow\infty)-\tilde{H}_I(\Delta k=0)$ and plotted in Fig. 5(b). The typical laser powers were 60 mW for the writing beam and 600 μW for the reading beam. The dashed and solid lines in Fig. 5(a) are calculated curves from Eqs. (16) and (17). At the early stage of the hole burning, where the writing time is $T_W\leqslant 25$ s, the hole depth increased, while the depth saturated and decreased after the irradiation of $T_W\geqslant 25$ s. This time development is in good accordance with the theory. The maximum hole depth observed in the type I sample was 0.17, which is somewhat small compared with the theoretical prediction. In order to compare the hole shape and the hole width in the early and the final stages of the experiment, the holes were normalized and plotted in Fig. 6(a). The solid and dashed lines are holes at $T_W=5$ s and $T_W=240$ s, respectively. The solid squares in Fig. 7 show the hole width $\Gamma_{\Delta k}$ as a function of the writing time. We see that the hole shape and width are unchanged within the error during the experiment in the type I sample. This dependence is in accordance with Eq. (15). Even if the photoreaction in the writing process is saturated, the correlation function that determines the hole shape is the lowest order of the intensity correlation between the writing and the reading beams, as long as the reading beam is weak enough to ignore the saturation effect.

Next, we examined the type II sample. Figure 8(a) shows luminescence intensity as a function of ΔkL in the type II sample in the reflection geometry. We see a clear hole in the luminescence intensity as a function of ΔkL. Figure 9 shows the luminescence intensities at the hole center $\tilde{H}_{II}(\Delta k=0)$ and at the background level $\tilde{H}_{II}(\Delta k\rightarrow\infty)$ as a function of the writing time. The behavior is almost similar to that of the type I sample. That is, in the early stage, the hole depth increased and then the depth saturated and decreased after an irradiation of $T_W\geqslant 100$ s. A difference between the type I and type II samples is seen in the initial stage. In Fig. 7, we also plotted the experimentally observed hole width in the type II sample by open circles. In the type II sample, the hole width became slightly narrower in the initial stage. This narrowing is explained by the luminescence reduction from the small z region as is discussed in Sec. III. The dashed line in Fig. 7 is calculated from Eq. (18). The experimental hole width at the early time shows a slight deviation from the calculated line. This discrepancy may arise because the dye concentration in our type II sample is not low enough to satisfy the condition $L_a\gg L$, and the hole width weakly shows characteristics relevant to the type III sample.

Finally, we examined the type III sample. Figure 8(b) shows the time development of the hole in the Δk domain in the type III sample in the reflection geometry. In Fig. 10, we plotted the luminescence intensities at the hole center $\tilde{H}_{III}(\Delta k=0)$ and at the background level $\tilde{H}_{III}(\Delta k\rightarrow\infty)$ as a function of the writing time. In Fig. 6(b) the normalized holes at the initial and the final stages are plotted. The time development in the type III sample is strikingly different from those of the type I and type II samples. The hole width is initially broad and becomes substantially narrower with increasing writing time. The normalized hole width $\Gamma_{\Delta k}$ as a function of the writing time is plotted in Fig. 7 by solid circles together with the experimental data of the type I and type II samples. In the type III sample, the absorption changes and the local speckle pattern also changes under the time development of the hole. The initial width could reflect the diffusive absorption length L_a, while the final hole width

reflects the sample thickness L. The maximum hole depth experimentally observed was 0.20 in the type III sample.

V. CONCLUSION

In conclusion, we investigated the time development of the hole burning in photoreactive and multiple-scattering media on the basis of the correlation between the local population and the local intensity of the reading beam. The development of the hole shape, width, and depth reflects the statistical fluctuations in the local speckle intensity. The maximum hole depth is ~ 0.26. The theoretical analyses were confirmed in the experiments in three types of multiple-scattering media which contain photochromic dyes as the photoreactive material.

ACKNOWLEDGMENTS

The authors are grateful to Dr. T. Ito for his cooperation in the early stage of the experiment. The authors are also grateful to Professor R. Matsushima for advice on photochromic dyes.

[1] J. C. Dainty, *Laser Speckle and Related Phenomena* (Springer-Verlag, Berlin (1984).
[2] *Scattering and Localization of Classical Waves in Random Media*, edited by P. Sheng (World Scientific, Singapore, (1990).
[3] A. A. Chabanov, M. Stoytchev, and A. Z. Genack, Nature (London) **404**, 850 (2000).
[4] A. A. Chabanov and A. Z. Genack, Phys. Rev. Lett. **87**, 153901 (2001).
[5] B. Spivak and A. Zyuzin, Phys. Rev. Lett. **84**, 1970 (2000).
[6] V. Emiliani, F. Intonti, M. Cazayous, D. S. Wiersma, M. Colocci, F. Aliev, and A. Lagendijk, Phys. Rev. Lett. **90**, 250801 (2003).
[7] T. Ito and M. Tomita, Phys. Rev. E **69**, 036610 (2004).
[8] S. Arnold, C. T. Liu, W. B. Whitten, and J. M. Ramsey, Opt. Lett. **16**, 420 (1991).
[9] M. Tomita, T. Ito, and S. Hattori, Phys. Rev. B **64**, 180202 (2001).
[10] A. Kurita, Y. Kanematsu, M. Watanabe, K. Hirata, and T. Kushida, Phys. Rev. Lett. **83**, 1582 (1999).
[11] *Spectroscopy and Excitation Dynamics of Condensed Molecular Systems*, edited by V. M. Agranovich and R. M. Hochstrasser (North-Holland, Amsterdam, 1983).
[12] S. Feng, C. Kane, P. A. Lee, and A. D. Stone, Phys. Rev. Lett. **61**, 834 (1988).
[13] R. Loudon, *The Quantum Theory of Light* (Oxford University Press, London, 1983).
[14] Makoto Tomita and Masahiro Matsuoka, J. Opt. Soc. Am. B **7**, 1198 (1990).